Grain Size Effects in the Quasi-Static Fracture Resistance of a Thermally Embrittled RPV Steel (Annealed Microstructures)

J.R. Tarpani, W.W. Bose Filho, and D. Spinelli

(Submitted 11 February 2002)

The elastic-plastic fracture toughness and crack extension behavior under quasi-static loading regimes of the as-received and several thermally embrittled states of a reactor pressure vessel (RPV) steel were assessed on the basis of microstructural parameters. Through a simple rule of mixture that is typically applied for composite materials, it was found that the equivalent grain size (EGS) of dual-phase annealed microstructures is the controlling parameter of the fracture properties. It was concluded that a Hall-Petch type relationship correlates the J-fracture mechanics criteria to the EGS.

Keywords fracture toughness, Hall-Petch relationship, J-R curve, neutron damage simulation, RPV steel

1. Introduction

In the last decade, there has been a great deal of research into the simulation of the mechanical behavior of structural steels submitted to neutron-dose damage in radioactive environments (e.g., reactor pressure vessel (RPV) steels), in particular if a crack-like singularity exists (i.e., by fracture mechanics concepts).[1-7] Considering the high risk and cost inherent to the manipulation of materials in the irradiated state, simulation techniques have obvious safety and economic motivations, since they would allow the development of new experimental procedures in nonradioactive environments and would make feasible prototype and full-scale vessel hydrotests, which so far never have been attempted in as-irradiated materials. The simulation of irradiation damage effects on the mechanical behavior of metallic alloys consistently has been tried by heat[1-6] and/or thermomechanical[7] treatments. However, only a few of these studies have made reference to the effect of microstructural variables such as grain size and phase percentage, especially in quantitative terms, on the mechanical performance of materials.

In this study, a nuclear-grade steel was submitted to annealing heat treatments that were aimed at obtaining a wide range of elastic-plastic fracture toughness levels in the quasi-static loading regime in order to evaluate quantitatively the microstructural parameters that control the fracture mechanisms acting on the different grades of embrittlement. The additional microstructures obtained from quenching and tempering the same low-alloy steel are currently under analysis, and the results will be presented elsewhere.[8]

J.R. Tarpani, W.W. Bose Filho, and **D. Spinelli,** Materials, Aeronautical and Automotive Engineering Department-SMM, Engineering School of São Carlos-EESC, University of São Paulo-USP, Av. Trabalhador São-Carlense, 400, São Carlos-SP, 13566-590-Brazil. Contact e-mail: jrpan@sc.usp.br.

2. Base Material

The Brazilian ASTM A508 class 3A steel (chemistry in Table 1) is a typical reactor pressure vessel (RPV) material that is designed for the nuclear industry. Figure 1(a) shows a schematic drawing of the original heat treatment applied to the steel for the as-delivered condition. Figure 1(b) shows the resultant microstructure, which is composed of a ferrite matrix with finely dispersed granular carbides that is characteristic of bainite.[9,10] This microstructure exhibits a mean grain diameter of 19 μm (8.5 micrograin ASTM number).

3. Experimental and Analytical Procedures

3.1 Annealing Thermal Cycles

Figure 2(a) shows schematic drawings of the seven embrittling heat treatments, designated B to H, that were individually applied to the A508 steel and are composed by an assortment of soaking times and temperatures.

3.2 Mechanical Properties and Fracture Toughness Test

Hardness measurements at ambient temperatures and tensile testing at 300 °C were carried out for the base and thermally embrittled materials.

Fracture mechanics J-R curve testing was performed via the unloading elastic compliance (UEC) technique under clip-gage-controlling elastic unloadings, in a computer-controlled, closed-loop, servohydraulic machine. For this purpose, miniaturized 5 mm and 10 mm thick compact tensile specimens (C[T]) were machined from the one-quarter-thickness position (T/4) of the as-received and thermally embrittled forged plates in transverse-longitudinal (T-L) orientation. Next, the specimens were precracked and side-grooved (SG) to 20% and 33% of their gross-thickness B_G and were tested at 300 °C, a typical operational RPV temperature, under a cross-head speed of 0.3 mm/min. Tests were stopped when the load dropped to 50% of the maximum load capacity of the specimens. Unloadings were limited to 15% of the current load in order to avoid fatigue crack growth and influences on J values.[11,12] J-Δa data points were obtained according to the ASTM E1820 standard,[13] (i.e.,

they were corrected for crack growth). Initial and final crack length predictions by elastic compliance measurements loosely satisfied the minimum accuracy requirements established by ASTM. Power-law fit then was applied to the J-Δa data points located within the limits of the validity of deformation-J (J_D) concept. In this study, these limits were defined by two exclusion offset lines at respectively 0.15 and 1.5 mm of crack growth, such as are typically used in determining crack initiation values.[13] Due to the reduced size of the specimens, it was verified that the maximum admissible -Δa (Δa_{max}) percentage according to the 1.5 mm exclusion line is roughly equivalent to that for J-R curves currently established as the ASTM standard, on the basis of the original ligament length percentage ($\Delta a_{max} = 0.25\ b_0$). Once traced, the J-crack resistance (J-R) curves, the J value for crack initiation (J_i or J_{IC}, if certain plasticity-constraining conditions in terms of J and specimen thickness are fulfilled, i.e., if the predominantly plane-strain conditions at the crack front are guaranteed), and the Paris & Johnson's crack instability criterion (J_{50}),[14] which is a well-known de-

Nomenclature

a, b, c, d, e, f	fitting constants
A, B, C, D, E, F, G, H	microstructures nomination
AC	air cooling
ASTM	American Society for Testing and Materials
b_0	original ligament length (mm)
B_G	gross thickness (mm)
BHN	Brinell hardness number
C[T]	compact tensile specimen
$dJ_{(D)}/d\Delta a$	rate of increase of J-crack growth resistance (kJ/m^2/mm)
$D_{bainite(ferrite)}$	mean diameter of bainite (ferrite) grain (μm)
D_0	original diameter (mm)
EGS	equivalent grain size (μm)
EL	elongation at fracture (%)
FC	furnace cooling
J	J-integral (kJ/m^2)
J_D	deformation J (kJ/m^2)
$J_i(J_{IC})$	initiation J (plane-strain) (kJ/m^2)
J-R	J-crack resistance curve
J-T_M	crack instability assessment diagram
J_{50}	Paris and Johnson's crack instability criterion (kJ/m^2)
L_0	original gage length (mm)
m	coefficient of power-law stress-strain relationship (MPa)
n	exponent of power-law stress-strain relationship
PWHT	post welding heat treatment
R	coefficient of correlation
RA	reduction in area at fracture
RPV	reactor pressure vessel
SG	side-groove level (%)
S_U	ultimate tensile strength (MPa)
S_Y	yield strength (MPa)
T	specimen or plate thickness
T-L	transversal-longitudinal orientation
T_M	tearing modulus
UEC	unloading elastic compliance
WQ	water quenching
$\Delta a_{(max)}$	(maximum) ductile crack growth (mm)
ε	engineering or nominal strain (%)
σ	engineering or nominal stress (MPa)

Table 1 Chemical Composition of the A508 Nuclear Grade Steel (wt.%)

C	Si	Mn	Ni	Mo	Cr	Al	P	S
0.19	0.24	1.30	0.72	0.51	0.03	0.012	0.007	0.009

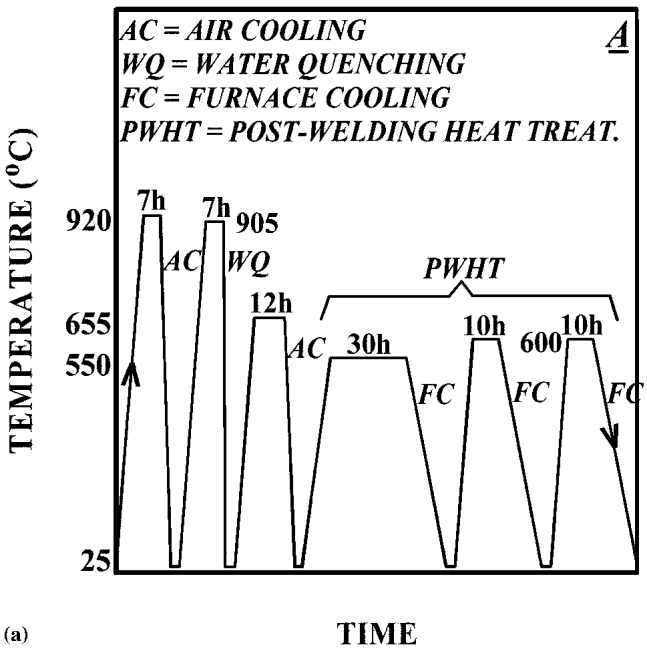

(a)

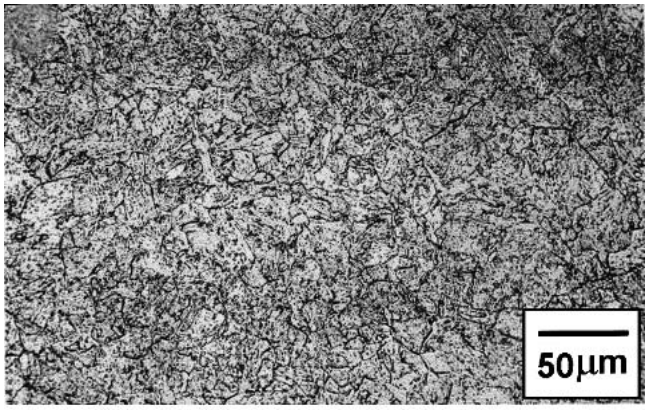

(b)

Fig. 1 (**a**) Schematic drawing of the fabrication thermal cycles for the A508-3A RPV steel; (**b**) as-received microstructure (A) exhibiting granular or globular bainite (nital etch)

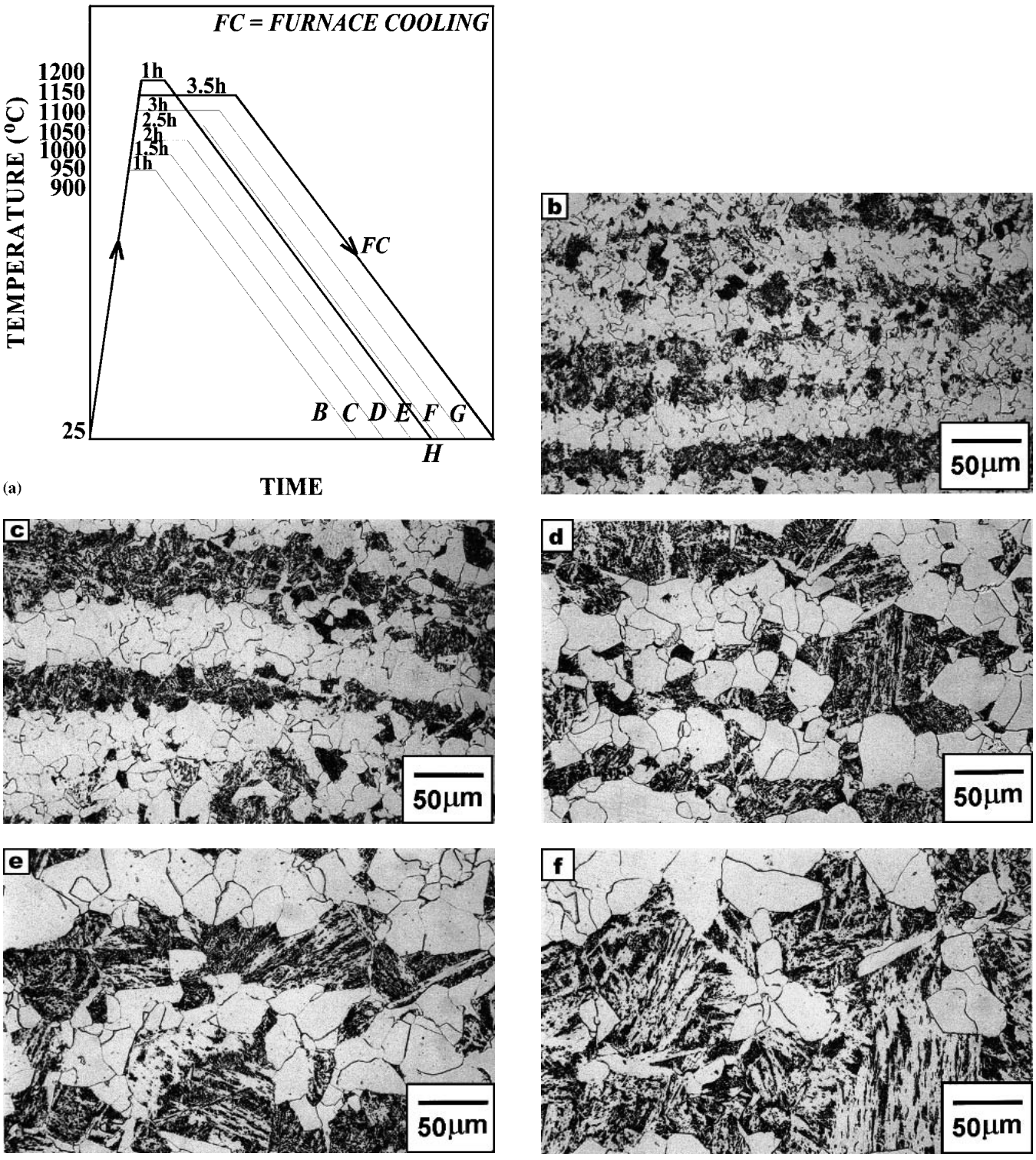

Fig. 2 (**a**) Schematic drawing of annealing routes applied to the original A508 steel (A); and (**b**) light micrographs of embrittled microstructures B (**c**) C, (**d**) D, (**e**) E, (**f**) F (continued on next page)

sign criterion against the tearing instability of pressurized flawed components, were determined. The J_i value was conventionally obtained at the intersection of the fitted J-R curve with the 0.2 mm offset line,[13] whereas the J_{50} criterion was determined following the J_{50} procedure on the space of crack instability assessment diagram (J-T_M), where T_M is the tearing modulus.[14] A third fracture toughness index,[15] namely, the rate of increase on the resistance to crack growth ($dJ_D/d\Delta a$) at 1 mm of crack propagation, then was derived. As a general rule, three J-testpieces were tested for each testing condition, so

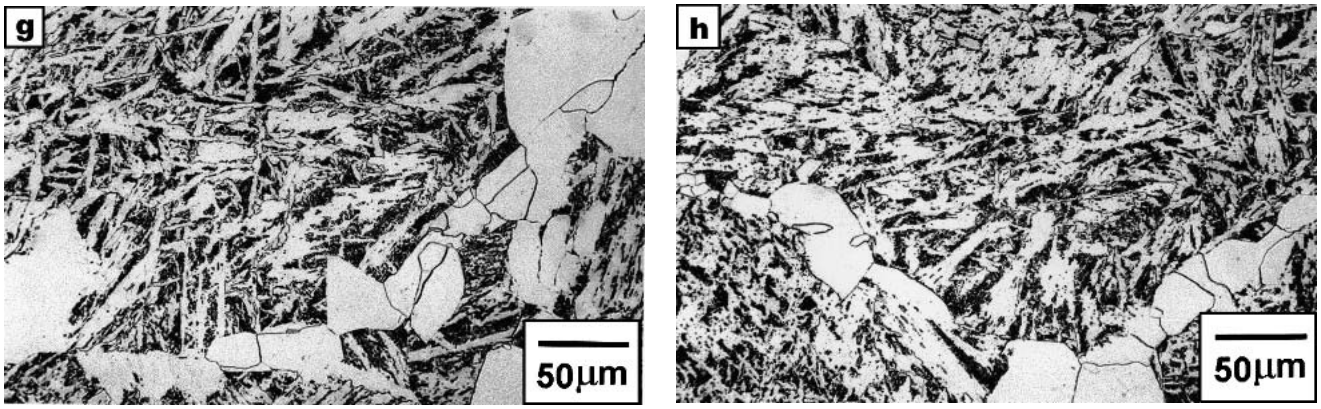

Fig. 2 cont. (**a**) Schematic drawing of annealing routes applied to the original A508 steel (A); and (**b**) light micrographs of embrittled microstructures B (**c**) C, (**d**) D, (**e**) E, (**f**) F, (**g**) G, and (**h**) H (nital etch)

Table 2 Microstructural Parameters and Phase Percentage of Tested Materials (a)

Annealing Route	$D_{ferrite}$, μm	$D_{bainite}$, μm	Phase, %	
			Ferrite	Bainite
B	20 (8.3)	19 (8.5)	48	52
C	30 (7.2)	26 (7.6)	49	51
D	39 (6.4)	50 (5.7)	50	50
E	47 (5.9)	56 (5.4)	50	50
F	50 (5.7)	64 (5.0)	51	49
G	55 (5.4)	475 (0)	19	81
H	61 (5.1)	817 (00)	11	89

(a) ASTM micrograin size number is provided in brackets.

that the results of J_i, J_{50}, and $dJ_D/d\Delta a$ at 1 mm measurements refer to the mean values.

4. Results and Discussion

4.1 Microstructural Characterization

Figures 2(b) to (h) present the annealed microstructures evaluated in this study. Basically, they comprise a mixture of nearly equiaxial grains of ferrite and globular low-carbon bainite. The mean grain diameters and phase percentages were determined by using a computerized image analyzer. Table 2 shows that, as expected, both ferrite and bainite grains grow with the annealing severity (B → H), but a quite outstanding acceleration on bainite grain growth is noticed for the G and H microstructures. It can be seen that milder annealing cycles generate both phases in a fixed proportion of about 1:1, but in microstructures G and H there exists far more bainite than ferrite. Higher austenitization temperatures, providing a larger prior austenite grain size in these microstructures, gave rise to higher hardenabilities, thus preventing the nucleation of the proeutectoid ferrite phase during furnace cooling. In this regard, a tradeoff between grain growth and microstructural refinement, the latter denoted by the acicularization of the bainite phase, is to be expected as the austenitization temperature is increased. Banding is observed to decrease with the degree of severity of the annealing heat treatment (i.e., along with the bainite refinement and grain growth). It is worthy of note that the thermal conditions leading to the loss of banding in microstructures G and H produced in a very unusual arrangement between the bainite and ferrite phases. Large grains of the former are completely surrounded by a network of relatively much smaller grains of the latter, which exhibit a very broad grain size distribution.

4.2 Hardness and Tensile Properties

Table 3 lists the conventional mechanical properties of the tested materials. Figure 3 displays the tensile flow curves of the materials to the maximum load capacity, according to the following power-law behavior model:

$$\sigma = m \cdot \varepsilon^n \quad \text{(Eq 1)}$$

where σ and ε are, respectively, the nominal or engineering stress and strain, and m and n are fitting constants (values for the latter are supplied in Table 3).

From Table 3, it can be observed that among all the conventional mechanical properties of the tested materials, only the reduction in area at fracture (RA) discloses unequivocally the decrease on fracture toughness of the materials, as the annealing severity is incremented from microstructures B to H. Furthermore, RA exhibits an inverse correlation to the granulometry of both phases found in all the annealing products (see Table 2), resembling a Hall-Petch type of relationship[16,17] in which the mechanical property varies inversely to the squared grain size.

Considering the dual-phase nature of the thermally embrittled materials, one can define a representative parameter for their composed granulometry. By means of a simple model, which is based on the rule of mixture typically applied for composite materials, an equivalent grain size (EGS) can be established. The EGS value must be a volume-fraction weighted average of the grain sizes of both individual phases (i.e., ferrite and bainite), and it is proposed as follows:

$$EGS = ((D_{ferrite}) \cdot (\%\ \text{ferrite}) + (D_{bainite}) \cdot (\%\ \text{bainite}))/100 \quad \text{(Eq 2)}$$

where the ferrite and bainite grain sizes, $D_{ferrite}$ and $D_{bainite}$, respectively, are furnished in Table 2 along with phase percentages.

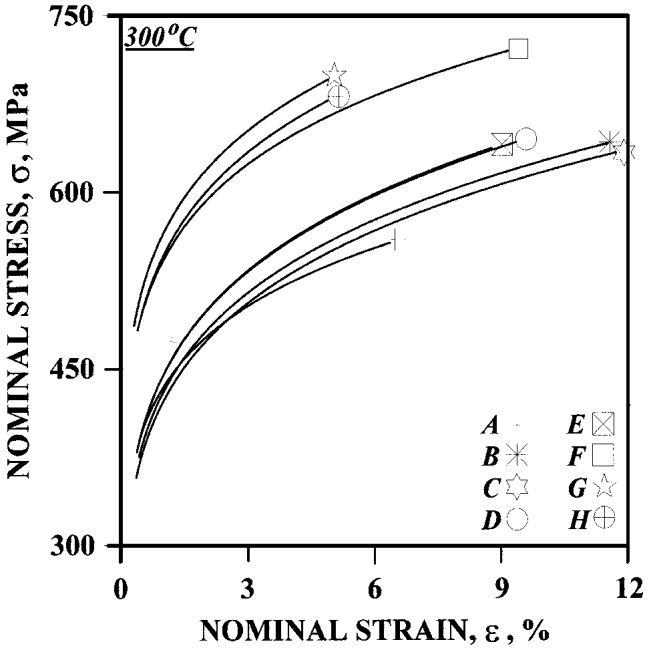

Fig. 3 Power-law stress-strain relationship according to Eq 1

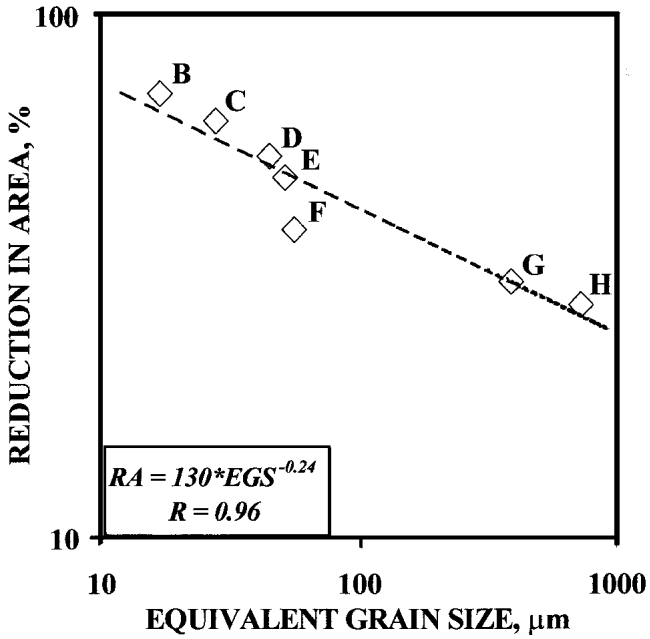

Fig. 4 Relationship between EGS and RA, according to Eq 3

Table 3 BHN and Tensile Properties of the As-Received and Thermally Embrittled Materials

Material	BHN, 100 kgf	S_Y, MPa	S_U, MPa	*n*	EL (a), %	RA, %
A	175	400	555	0.15	11	77
B	170	360	620	0.17	17	71
C	167	345	610	0.17	16	63
D	168	370	620	0.17	12	54
E	169	375	625	0.17	12	49
F	192	450	675	0.11	11	39
G	198	470	685	0.14	05	31
H	208	490	665	0.14	05	28

(a) $L_0 \cong 40$ mm $\cong 10\ D_0$.

Figure 4 displays, in logarithmic scales, a good data correlation between RA and EGS, as denoted by the high correlation coefficient (R). A power-law relationship, similar to that of Hall-Petch, is established as follows:

$$RA = a \cdot EGS^{-b} \quad \text{(Eq 3)}$$

where *a* and *b* are fitting constants.

This relationship indicates that RA is driven by grain size rather than controlled by the concurrent microstructural (bainite) refinement. Later in this article, the same dependence will be shown concerning fracture toughness properties.

4.3 J-R Curves and Fracture Toughness Criteria

Figure 5 presents typical J-Δa data points experimentally determined for all the states of the A508 steel, in which extensive ductile crack growth is verified, typically in the range of 2.5-4 mm.

Except for microstructures D and H, it can be observed that the rank established for RA, in terms of EGS (see Fig. 4), is faithfully obeyed for the J-R curves positioning, signaling that EGS also controls the ductile crack growth resistance of the materials.

The unexpected slightly better performance of microstructure D over that of C, on the basis of the EGS concept, can possibly be explained by the major role eventually played by bainite refinement than grain growth, regarding both fracture toughness and crack extension behavior.

Concerning microstructure H, the anomalous behavior of the J-Δa data in presenting a sigmoidal arrangement is quite noticeable and prevented all J-fracture toughness criteria from being determined. This effect is probably due to the development of cumulative fatigue damage during the precracking procedure, when fatigue microcracking spread into the fracture process zone at the crack tip, thus excessively embrittling the material and, consequently, leading to a very poor resistance to crack propagation in the very first stages of J-R curve testing. We return to this point in a companion article[8] regarding quenched and tempered microstructures that are prone to cracking in a brittle and intergranular manner, which were also invariably related to coarser grain microstructures.

By comparing Fig. 5(a) and (b), it is observed that, as expected, a deeper SG level produces more conservative J-R curves due to higher plastic constraint, i.e., more predominant stress triaxility along the crack leading edge. Also, a slight J-specimen size dependence for the microstructure G is noticed in Fig. 5(b), in which the thinner testpiece gives a less conservative J-R curve as a consequence of the loss of plastic constraint (i.e., stress relaxation along the crack front).

Given the reduced size of the testpieces, only the 10 mm thick specimen that is correspondent to microstructure G fulfilled both the maximum J-capacity and minimum thickness requirements established in Ref. 13 regarding the qualification of the initiation J value as a truly J_{IC} criterion.

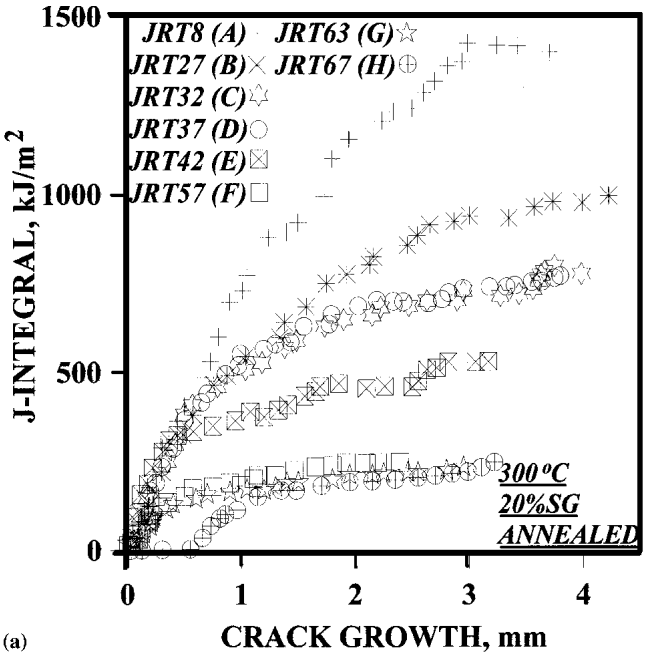

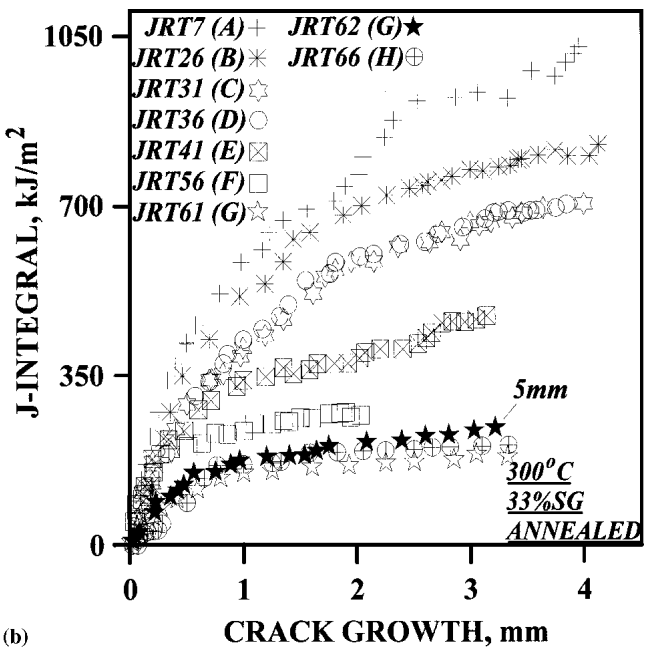

Fig. 5 Typical J-Δ*a* curves of tested materials. (**a**) 20% SG; and (**b**) 33% SG test specimens. Testpieces are 10 mm thick unless otherwise indicated. J-R curves of the original A508 steel are supplied as a baseline.

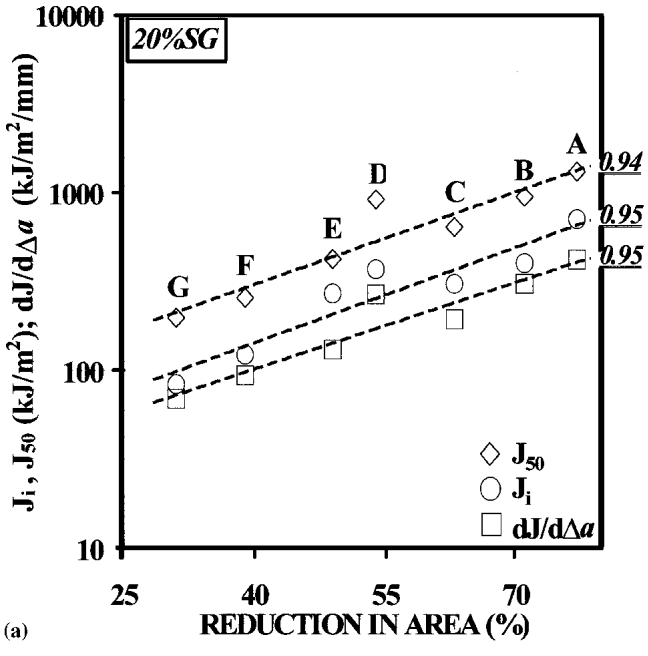

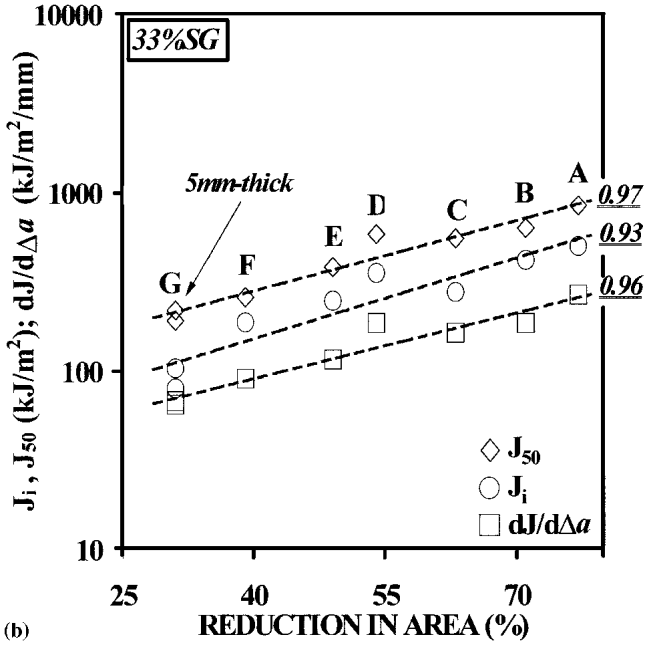

Fig. 6 Relationship between all the J-criteria and RA, according to Eq 4. (**a**) 20% SG test specimen, and (**b**) 33% SG test specimen. Test specimens are 10 mm thick unless otherwise specified.

Figure 6 displays, in logarithmic scale, the relationships between RA and all the J-based fracture toughness criteria, namely, J_i, J_{50}, and $dJ_D/d\Delta a_{(1mm)}$. It can be seen that, with no exceptions, the data correlate fairly well. This is especially verified for the highest crack tip constraining condition (i.e., the deepest SG level). The J-based criteria obey an exponential law regarding RA, which is given by:

$$J = c \cdot \exp^{(d \cdot RA)} \quad \text{(Eq 4)}$$

where c and d are fitting constants.

Interestingly, microstructure A fits well with annealed ones regarding J-criteria versus RA relationships. This is probably due to the heavy tempering imposed on this material during the postwelding heat treatment (PWHT) simulation (Fig. 1), which render to it an annealed-like behavior during tensile tests.

The above figures indirectly establish the dependence of all J-criteria with the EGS concept, as long as RA already has been proven to strongly depend on that parameter (see Fig. 4). In Fig. 7, this expected dependence of J-criteria on EGS is given,

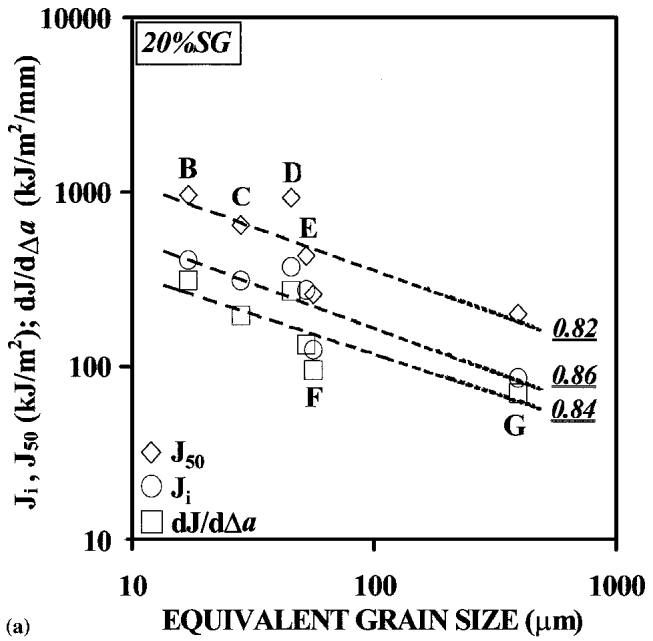

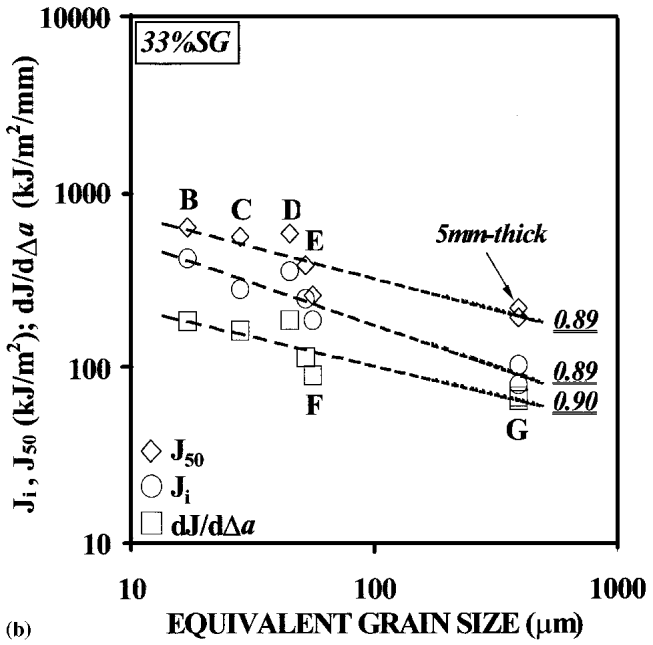

Fig. 7 Relationship between all the J-criteria and EGS, according to Eq 5. (**a**) 20% SG test specimen, and (**b**) 33% SG test specimen. Test specimens are 10 mm thick unless otherwise specified.

Table 4 Exponent *f* From the Power-Law Dependence of J-Based Parameters With Equivalent Grain Size According to Eq 5.

	f Testpiece SG Level	
Fracture Toughness Index	**20%**	**33%**
J_{50}	0.499	0.425
J_i	0.513	0.480
$dJ_D/d\Delta a$ (1mm)	0.470	0.405

in logarithmic scales, according to a Hall-Petch power law type of relationship, as follows:

$$J = e \cdot EGS^{-f} \quad \text{(Eq 5)}$$

where e and f are fitting constants.

Table 4 lists the values of the exponent f in Eq 5 for all the cases analyzed in this study. Given the simplicity of the adopted model of the rule of mixture for deriving the EGS concept, the f values may be considered to be quite good approximations of the well-known 0.5 exponent of Hall-Petch.

A correlation between the properties of elastic-plastic fracture mechanics and grain size of single-phase metallic materials has been proposed in literature,[18,19] invariably on the basis of the widely accepted Hall-Petch relationship. The present study has shown that the same principle could be applied to dual-phase, structural, low-alloy steels, as long as the EGS concept is taken from the well-known rule of mixtures, which is typically proposed for composite materials.

5. Conclusion

The elastic-plastic fracture toughness and crack extension behavior under a quasi-static loading regime of the as-received and of several thermally embrittled states of a nuclear RPV steel were assessed on the basis of microstructural parameters. By using a simple rule of mixture, it was concluded that the EGS concept of dual-phase annealed microstructures is the controlling parameter of fracture properties. The procedure was based on the relative percentage of the phases present in the thermally embrittled microstructures, which was similar to that proposed for the inference of the mechanical properties of composite materials. The dependence of fracture properties on grain size was shown to be a Hall-Petch type of relationship, which so far has been proven only in single-phase metals and alloys. Also, this study determined that the RA obtained from tensile testing correlates fairly well with several J-fracture toughness criteria as applied to structural integrity assessment in the nuclear industry. The same analysis has been extended to quenched and tempered microstructures obtained from the same low-alloy steel and will be reported on in a companion article.

Acknowledgment

The authors are grateful to Funda ção para o Amparo à Pesquisa do Estado de São Paulo (FAPESP) (contract 97-05652/1) for financial support.

References

1. K. Onizawa, K. Fukaia, Y. Nishiyama, M. Suzuki, S. Kaihara, and T. Nakamura: "Development of a Reconstitution Technique for Charpy Impact Specimens by Surface-Activated Joining for Reactor Pressure Vessel Surveillance," *Int. J. Press. Vessels Piping*, 1997, *70*, pp. 201-07.
2. V.V. Pokrovsky, V.T. Troshchenko, V.G. Kaplunenko, V.Y. Podkol'zin, V.G. Fiodorov, and G. Dragunov: "A Promising Method for Enhancing Resistance of Pressure Vessels to Brittle Fracture," *Int. J. Press. Vessels Piping*, 1994, *54*, pp. 9-24.
3. H. Hanninen: "Phenomena of Material Degradation with Time Rel-

evant to Reactor Pressure Vessels," *Int. J. Press. Vessels Piping*, 1993, *54*, pp. 9-30.
4. I.A. Vatter, C.A. Hippsley, and S.G. Druce: "Review of Thermal Aging Data and its Application to Operating Reactor Pressure Vessels," *Int. J. Press. Vessels Piping*, 1993, *54*, pp. 31-48.
5. B.T. Timofeev, V.A. Petrov, G.P. Karzov, and V.V. Anikovsky: "Methods for the Evaluation of Crack Resistance of Reactor P.V. Materials under Conditions of Thermal Shock," *Int. J. Press. Vessels Piping*, 1992, *52*, pp. 159-75.
6. E. Vitale and M. Beghini: "Thermal Shock Fracture Experiments on Large Size Plates of A533-B Steel," *Int. J. Press. Vessels Piping*, 1991, *46*, pp. 289-338.
7. G. de Diego, Ma.L. Castaño, and M. Hernández: "Simulación del Efecto de la Irradiación Mediante el Trabajado en Frío y los Tratamientos Térmicos en los Aceros Inoxidables Austeníticos," *Rev. Metall.*, 1998, *34*, pp. 407-20 (in Spanish).
8. J.R. Tarpani, W.W. Bose Filho, and D. Spinelli: "Grain Size Effects in the Quasi-Static Fracture Resistance of a Thermally Embrittled RPV Steel (Annealed Microstructures)," *J. Mater. Eng. Perform.,* 2002, *11*(4), pp. 414-21.
9. L.B. Bramfitt and J.G. Speer: "A Perspective on the Morphology of Bainite," *Metall. Trans.*, 1990, *21A*, pp. 817-29.
10. D.V. Edmonds and R.C. Cochrane: "Structure-Property Relationships in Bainitic Steels," *Metall. Trans.*, 1990, *21A*, pp. 1527-40.
11. S. Kaiser: "On the Relation Between Stable Crack Growth and Fatigue," *Fatig. Eng. Mater.*, 1983, *6*, pp. 32-38.
12. K. Krompholz and G. Ullrich: "Determination of J-integral R-curves for the Pressure Vessel Material A533 B1 Using the Potential-Drop Technique and the Multispecimen Method," *Eng. Fract. Mech.*, 1986, *23*, pp. 803-20.
13. Anon.: "ASTM Designation E1820-Standard Test Method for Measurement of Fracture Toughness," *Annual Book of ASTM Standards*, ASTM, Philadelphia, PA, 1997.
14. P.C. Paris and R.E. Johnson: "A Method of Application of Elastic-Plastic Fracture Mechanics to Nuclear Vessels Analysis," *ASTM STP*, 1983, *803*, pp. 5-40.
15. E.M. Hackett and J.A. Joyce: "Use of J-R Curves in Assessing the Fracture Behavior of Low Upper Shelf Toughness Materials," *Nucl. Eng. Design*, 1992, *134*, pp. 217-26.
16. N.J. Petch: "The Cleavage Strength of Polycrystals," *J. Iron Steel Inst.*, 1953, *174*, pp. 25-28.
17. E.O. Hall: "The Deformation and Ageing of Mild Steel," *Proc. Phys. Soc. B.*, 1951, *64*, pp. 747-53.
18. M. Srinivas, G. Malakondaiah, R.W. Armstrong, and P.R. Rao: "Ductile Fracture Toughness of Polycrystalline Armco Iron of Varying Grain Size," *Acta Metall. Mater.*, 1991, *39*, pp. 807-16.
19. M. Srinivas, G. Malakondaiah, R.W. Armstrong, and P.R. Rao: "Influence of Polycrystal Grain Size on Fracture Toughness of and Fatigue Threshold in Armco Iron," *Eng. Fract. Mech.*, 1987, *28*, pp. 561-76.